JOURNAL OF GEOPHYSICAL RESEARCH, VOL. 106, NO. B7, PAGES 13,581–13,597, JULY 10, 2001

Spatial extent of a hydrothermal system at Kilauea Volcano, Hawaii, determined from array analyses of shallow long-period seismicity 2. Results

Javier Almendros, Bernard Chouet, and Phillip Dawson
U.S. Geological Survey, Menlo Park, California

Abstract. Array data from a seismic experiment carried out at Kilauea Volcano, Hawaii, in February 1997, are analyzed by the frequency-slowness method. The slowness vectors are determined at each of three small-aperture seismic antennas for the first arrivals of 1129 long-period (LP) events and 147 samples of volcanic tremor. The source locations are determined by using a probabilistic method which compares the event azimuths and slownesses with a slowness vector model. The results show that all the LP seismicity, including both discrete LP events and tremor, was generated in the same source region along the east flank of the Halemaumau pit crater, demonstrating the strong relation that exists between the two types of activities. The dimensions of the source region are approximately $0.6 \times 1.0 \times 0.5$ km. For LP events we are able to resolve at least three different clusters of events. The most active cluster is centered ~200 m northeast of Halemaumau at depths shallower than 200 m beneath the caldera floor. A second cluster is located beneath the northeast quadrant of Halemaumau at a depth of ~400 m. The third cluster is <200 m deep and extends southeastward from the northeast quadrant of Halemaumau. Only one source zone is resolved for tremor. This zone is coincident with the most active source zone of LP events, northeast of Halemaumau. The location, depth, and size of the source region suggest a hydrothermal origin for all the analyzed LP seismicity.

1. Introduction

Kilauea Volcano, Hawaii (Figure 1), is one of the best studied volcanoes in the world. The low risk presented by its typical eruptions, its high level of activity, and its easy access have contributed to make it a preferred natural laboratory for volcanologists.

Nearly all known eruptions of Kilauea have taken place either within its summit caldera or along the rift zones [*Lockwood et al*., 1999]. Halemaumau crater was the site of nearly continuous lava lake activity from 1823 to 1923. However, following the disappearance of the lava lake and an ensuing series of phreatic eruptions in May 1924, the century-long sustained summit activity ceased. During the next 10 years, eruptive activity at Kilauea was sporadic and weak and was entirely restricted to Halemaumau. From 1935 to 1951, Kilauea was completely inactive. Between 1952 and the mid-1960s, numerous short-lived eruptions took place within the summit caldera. An 8-month-long eruption occurred in Halemaumau in 1967–1968; it marked the longest-duration activity at Kilauea since 1924 and exhibited sustained lava lake activity typical of the activity prevailing for the century prior to 1924. Beginning in 1969, however, eruptions in the East Rift Zone have dominated the activity at Kilauea. These include the 1969–1974 eruption at Mauna Ulu [*Swanson et al*., 1979; *Tilling*, 1987], and the Puu Oo eruption [*Wolfe*, 1988; *Heliker and Wright*, 1991], which began in 1983 and continues at the present. The last eruptive activity in the summit region occurred in 1972–1974 [*Lockwood et al*., 1999] and 1981–1983 [*Klein et al*., 1987].

Paper number 2001JB000309
0148-0027/01/2001JB000309$09.00

1.1. How Kilauea Works

Eaton and Murata [1960] first proposed a dynamic model of Kilauea whose basic features are still valid today. Later intensive studies of several eruptions using advanced geophysical techniques, including mainly seismic and geodetic measurements, contributed new insights to the 1960 model. At present, we have a global but rough understanding of how the volcano works [*Decker*, 1987; *Tilling and Dvorak*, 1993]. The origin of Kilauea, and other Hawaiian volcanoes, is generally attributed to the interaction between a hot spot in the mantle and the Pacific plate [*Wilson*, 1963; *Christofferson*, 1968; *Clague and Dalrymple*, 1987]. Magma rises from the mantle through a narrow pipe-like conduit located beneath the summit caldera. This conduit extends in depth from roughly 40 to 7 km [*Klein et al*., 1987]. Between 7 and 2 km, magma resides temporarily in a shallow reservoir made of a plexus of interconnected magma pockets and conduits, located predominantly beneath the southern part of the summit region [*Fiske and Kinoshita*, 1969]. From there, magma can be transferred to two rift zones extending to the east and southwest, respectively, by means of shallow, horizontal pathways at depths near 3 km [*Klein et al*., 1987]. Eruptions take place when the crust above these conduits splits open in response to magma pressurization.

1.2. Seismicity

Volcano seismicity shows different types of signatures, which may be attributed to two general source groups [*Chouet*, 1996].

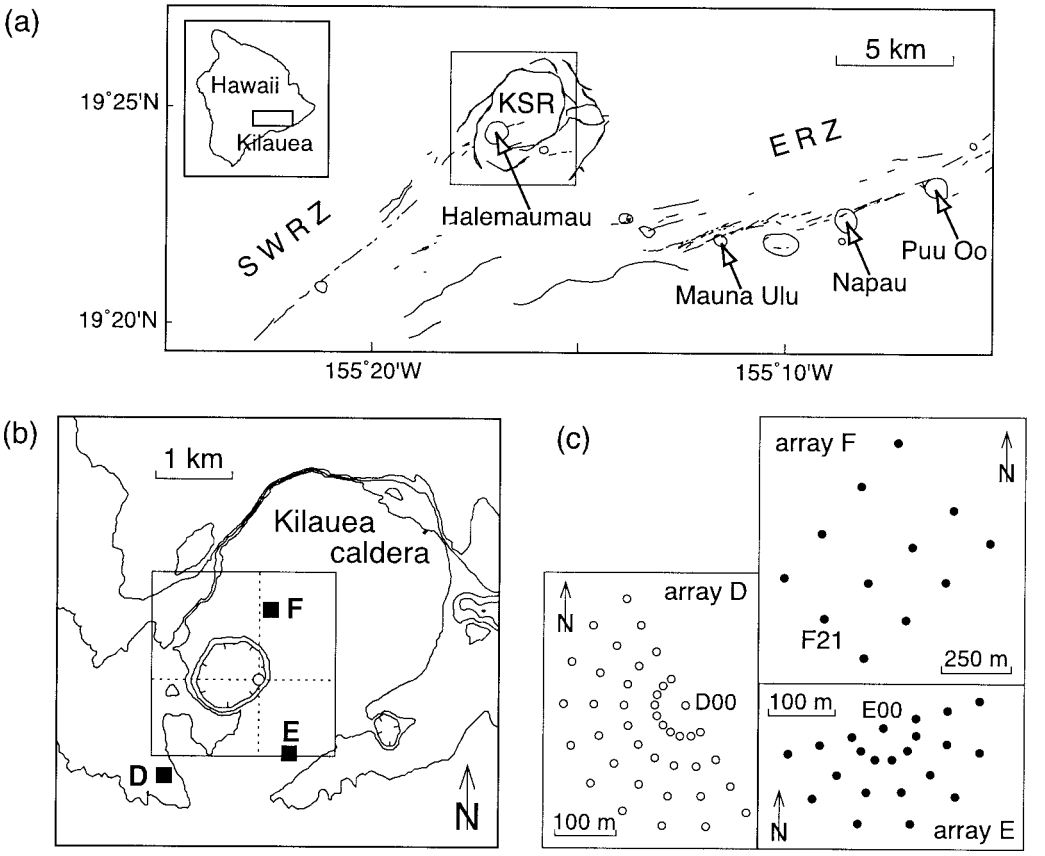

Figure 1. (a) Map of Kilauea, showing its location on the island of Hawaii (inset) and the locations of the Southwest and East Rift Zones (SWRZ and ERZ, respectively) and Kilauea summit region (KSR). The locations of several pit craters are indicated by arrows. The box around the summit region marks the area enlarged in Figure 1b. (b) Map of Kilauea caldera, showing the positions of the centers of the seismic antennas D, E, and F (solid squares). The contour interval is 40 m. The box outlines the area within which the slowness vector model was calculated (see text for explanations). The open circle marks the origin of the coordinate system used to locate LP events and tremor samples. (c) Configuration of the seismic antennas. Open circles are three-component stations, and solid dots are vertical component stations. Stations D00, E00, and F21, were selected to show the sample seismograms in Figures 2, 3, 4, 5, and 6.

The first group consists of volcano-tectonic (VT) earthquakes and represents shear or tensile sources involving brittle rock failure in response to variations of pressure in the magma reservoir and conduits. The second group consists of volumetric sources, in which the fluid is dynamically coupled with the surrounding rock, and elastic radiation is the result of pressure disturbances in the multiphase flow of magmatic and/or hydrothermal fluids through cracks and conduits. Volcanic tremor and long-period (LP) events are manifestations of such processes and are collectively referred to as LP seismicity [*Chouet*, 1996]. The spatial distributions of VT sources have been used to gain information about the stress state of volcanoes and to obtain rough maps of the magma transport and storage structures beneath volcanoes such as Kilauea [*Klein et al*., 1987; *Ryan et al*., 1981], Mount St. Helens [*Moran*, 1994], and Redoubt [*Lahr et al*., 1994].

At Kilauea, VT earthquakes are recorded to depths of >40 km [*Tilling and Dvorak*, 1993], broadly outlining the conduit followed by magma on its way to the surface. Volcanic tremor and LP events are usually grouped in three depth ranges based on the frequency content and amplitude attenuation pattern of the records obtained on the Hawaiian Volcano Observatory (HVO) network and, rarely, on locations of exceptionally impulsive LP events. These ranges are 30–60 km, 5–15 km, and <5 km [*Koyanagi et al*., 1987]. Within the summit region, shallow seismicity classified as caldera events by HVO is frequently observed. Because of the emergent character of the seismograms this seismicity cannot be located by conventional phase pick techniques.

1.3. Kilauea at the Time of This Study

Since the onset of the current Puu Oo eruption in January 1983, the summit region has been acting basically as a temporary storage region with noneruptive behavior. Ground tilt measurements show typical patterns of slow rise and rapid subsidence related to each eruptive episode. This pattern results from the rise of magma into the summit reservoir over the course of several months, followed by lateral movement of magma from the summit reservoir into the rift zone [*Tilling and Dvorak*, 1993], where an eruption occurs. Ground tilting correlates with the occurrence of VT earthquakes as the brittle cap over the magma reservoir extends and cracks and also with LP events as the system rapidly begins to refill from below [*Klein et al*., 1987].

In early February 1997, a joint Japan-U.S. experiment was conducted in Kilauea caldera to constrain the locations of the different types of sources, including both very long period (VLP) signals associated with magma flow and shallow caldera events recorded by the short-period HVO network. Three small-aperture (300, 400, and 700 m) seismic antennas were deployed around the Halemaumau pit crater for the specific purpose of tracking shallow LP seismicity. Small-aperture seismic antennas have been used to study the source of LP events and tremor in volcanic areas [*Goldstein and Chouet*, 1994; *Almendros et al*., 1997; *Chouet et al*., 1997; *Métaxian et al*., 1997; *Almendros et al*., 1999; *Del Pezzo et al*., 1999; *Ibáñez et al*., 2000; *Saccorotti et al*., 2001]. Such antennas have also been used to investigate the properties of tremor wave fields and to determine the shallow velocity structure beneath the antenna site [*Gordeev et al*., 1990; *Ferrazzini et al*., 1991; *Del Pezzo et al*., 1993; *De Luca et al*., 1997; *Chouet et al*., 1998].

At the time of the 1997 experiment, Kilauea Volcano was in a reinflation phase following a brief eruptive episode in Napau crater [*Chouet and Dawson*, 1997]. The Napau eruption occurred after a strong deflation (30 μrad) of the summit caldera on January 29–30, 1997. This deflation marked the end of episode 53 in the 17-year-long Puu Oo eruption. Geodetic surveys indicated extension along the East Rift Zone resulting from the rapid draining of the summit reservoir into the rift conduit, and on January 30, roughly 3×10^5 m^3 of lava were erupted from five fissures extending along a northeasterly line in the Napau crater area over a period of 22 hours. The eruption at Napau crater marked the termination of lava migration down rift. Over the following weeks, periods of inflation and minor deflation resulted in a net inflation of the Kilauea summit of $\sim$10 μrad. On February 11 a rapid inflation of $\sim$2 μrad was recorded by the summit tiltmeters. Following this event, the rate of summit inflation generally increased, interrupted by short periods of very minor deflation.

From February 8 through 12 the deployed instruments recorded a swarm of caldera events and tremor that had been going on since the strong deflation of the summit caldera at the end of January. Because of the emergent character of these signals, no hypocenter information was available prior to the summit experiments. The only clues as to the source location of this seismicity come from *Saccorotti et al*. [2001], who used array data recorded during a similar experiment carried out 1 year earlier in the same region [*McNutt et al*., 1997] to study the wave field properties of a LP event and volcanic tremor occurring beneath the summit of Kilauea. *Saccorotti et al*. [2001] found that both types of events were located beneath the northeast edge of Halemaumau. They determined a shallow origin (depth below surface $\sim$100 m) for the source of the LP event and a deeper origin (depth $\leq$1 km) for the source of tremor.

In this paper, we apply the method described by *Almendros et al*. [this issue] to seismic array data to determine the spatial location and extent of the source of the LP events and tremor recorded at Kilauea Volcano in February 1997 during the Japan-U.S. seismic experiment.

2. Experiment Setting and Instrumentation

The seismic instrumentation for this experiment included three seismic antennas deployed around the Halemaumau crater (arrays D, E, and F, Figure 1b). Array D, with an aperture of 400 m, featured 41 three-component seismometers deployed in a semicircular spoked pattern with a station spacing of 50 m along the spokes and angular spacing of 20° between spokes (Figure 1c). Array E had an aperture of 300 m and consisted of 22 vertical component seismometers deployed in a semicircular spoked pattern with a station spacing of 50 m along the spokes and angular spacing of 30° between spokes (Figure 1c). Array F had an aperture of 700 m and consisted of a sparse rectangular network of 12 vertical component seismometers (Figure 1c). Vertical component stations were equipped with Mark Products L11-4A sensors, and three-component stations featured Mark Products L22-3D sensors. All sensors had a natural frequency of 2 Hz and sensitivity of 50 V/(m/s). The data were sampled at 100 samples per second and recorded on 16-bit, three-channel Hakusan data loggers. All instruments used a common GOS time base with an accuracy of 5 μs among all the channels. Data were stored in a 20-MB flash memory that allowed continuous mode recording for up to 11 hours. The three antennas operated simultaneously during five 11-hour-long periods, producing $\sim$50 hours of synchronized data.

3. Data Description

The data analyzed in this paper are part of a swarm of LP activity that occurred at Kilauea Volcano during the first weeks of February 1997. The seismic antennas operated simultaneously 11 hours each day, from February 8 to 12. Several thousand events were recorded over a low-amplitude background of volcanic tremor. Figure 2 shows a 50-min sample of data representative of the seismicity of the volcano during the swarm.

The seismograms of shallow LP events are generally emergent, have a spindle-shaped amplitude envelope, and have typical durations in the range 10–40 s. The waveforms are coherent across the antennas but change drastically from antenna to antenna over distances of the order of 2–3 km. The spectral content is heterogenous both in time (from event to event) and space (from antenna to antenna). Such features are signs of path and/or site effects. The shape of the spectrum is relatively broad, occupying the 1–15 Hz band (Figure 3) with dominant peaks in the range 2–6 Hz. The appellation long-period event is not fully appropriate in this particular case because the frequency of the main peak of these events can actually be high compared to the usual frequency content of LP events (0.5–5 Hz) at other volcanoes. Nevertheless, we use this name in reference to the presence of a resonant source mechanism, as demonstrated by *Saccorotti et al*. [2001] for a similar event recorded in 1996.

4. Frequency-Slowness Analyses

Our method for locating seismic events using antennas is based on estimates of the apparent slowness vectors of the wave fields. The directions of these vectors provide the propagation azimuths of the wave fields, whereas their moduli represent the inverses of the apparent propagation velocities of the waves across the antenna. We perform frequency-slowness analyses of antenna data using the MUSIC algorithm [*Schmidt*, 1986; *Goldstein and Archuleta*, 1987]. The details are fully described by *Almendros et al*. [this issue].

4.1. General Procedure

We selected 23 hours of array data. Nineteen of these hours correspond to the most active period of the seismic swarm

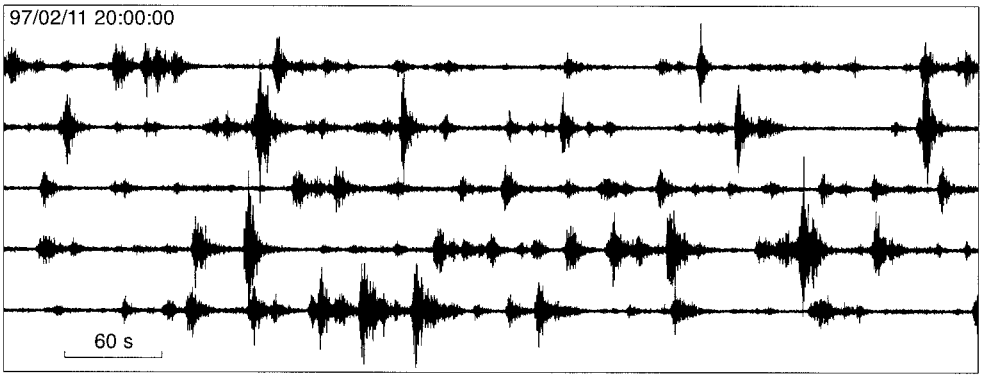

Figure 2. Sample showing 50 min of vertical component data recorded at station D00 (see Figure 1c) on February 11, 1997, starting at 2000 LT (Hawaiian Standard Time). A similar level of seismicity was observed during the rest of the analyzed LP swarm.

(February 11, 1900 LT to February 12, 0300 LT and February 12, 1300 LT to February 13, 0000 LT), and 4 hours represent a period of lesser but increasing activity during the 3 previous days (February 8, 2100–2200 LT, February 9, 0100–0200 LT, February 10, 1600–1700 LT, and February 11, 0100–0200 LT). All times used throughout this paper are Hawaiian Standard Time. Following a careful inspection of all the traces, noisy or troublesome channels were discarded, which left 36–41 sensors on antenna D, 19–22 sensors on antenna E, and 12 sensors on antenna F. All the selected records are vertical component seismograms. The raw data were corrected for offsets and filtered using a zero-phase, six-pole high-pass Butterworth filter with a corner frequency of 0.2 Hz. Frequency-slowness spectra were estimated in a 2.56-s-long window (256 samples) sliding in increments of 0.2 s along the records. The parameters used for our analysis are slightly different for arrays D, E, and F, owing to their different configurations. For data recorded on the D and E antennas we used 11 frequency bands with individual bandwidth of 1.2 Hz and overlap of 0.4 Hz, spanning the bandwidth 1–10 Hz. The investigated range of apparent slownesses was limited to values smaller than 2 s/km on these antennas. In array F, however, the stations are too sparsely distributed to consider such slow waves, especially at frequencies above 6 Hz, because of the lack of wave coherency across the array. For this array our analysis was limited to six frequency bands spanning 1 to 6 Hz, with a maximum slowness of 1 s/km. Using an uncertainty in time delays $\delta t = 0.05$ s and a signal-to-noise ratio $R = 10$, we obtain slowness resolutions of 0.05, 0.09, and 0.04 s/km for the D, E, and F antennas, respectively [*Goldstein and Archuleta*, 1991]. Keeping computation time in mind, we selected slowness grid spacings of 0.1, 0.1, and 0.05 s/km for the data processing at arrays D, E, and F, respectively. This yielded a slowness domain consisting of 41×41 nodes for each antenna. The number of signals selected was limited to 2. Therefore the signal subspace is defined by the eigenvectors corresponding to the two largest eigenvalues. In this paper, we only consider the primary peak corresponding to the dominant source in the wave field. The features of the secondary peak will be addressed in a future paper. Figure 4 shows slowness spectra obtained for a single 2.56-s window for a sample event recorded by array D. The position of the spectral peak is very stable in different frequency bands; however the coherence is higher at lower frequencies as indicated by higher values of the maximum power in the frequency-slowness spectra. The stacked slowness spectrum shows a narrow maximum, which yields a precise estimate of the slowness vector.

4.2. Analyses of LP Events and Tremor

The frequency-slowness analyses provide values of the propagation azimuth and apparent slowness, together with their error limits, in the form of time series with a sampling interval of 0.2 s. Using Matlab, we have designed a computer tool to scroll through this huge amount of data, so as to visualize and manage individual event analyses in an easy and flexible way. The code first displays the seismograms recorded over an extended window (1-hour long) at stations D00, E00, and F21 (see Figure 1c). In this window we can zoom to focus on one particular LP event or tremor sample. For LP events our selection was based on the visual character of the signals, mainly the signal-to-noise ratio. For tremor, we looked for sustained signals excluding LP events, with amplitude above the noise level. Finding pure tremor samples was difficult, especially during the most active part of the swarm, because LP events were then occurring at a fast rate of up to several events per minute. Most of the selected tremor samples belong to the first 4, quieter hours of analyzed data. Over the selected data interval, the frequency-slowness results are shown for each array, together with the corresponding seismograms recorded at D00, E00, and F21.

To locate the source of a LP event, we focus our attention on the results corresponding to the onset of the waves recorded by each array. We name this time interval the first-arrival window. Our criteria in selecting this window are (1) stability in the azimuth, that is, energy coming from the same direction for a reasonably long time, (2) high slowness power, indicative of good coherence between the traces, and (3) simultaneous presence of a window with similar characteristics at the other antennas to ensure that the event was caught by three antennas and that a joint location could be performed. A similar set of criteria was applied to select an arrival window in tremor records, except that in this case the selected arrivals are part of a sustained wave train and are not representative of a particular event onset.

Time series plots are made of stacked slowness power, azimuth, and apparent slowness. The most usual behavior observed in these plots during the first-arrival windows, although slightly different at each antenna, can be summarized by the following characteristics. For LP events a sharp jump in the

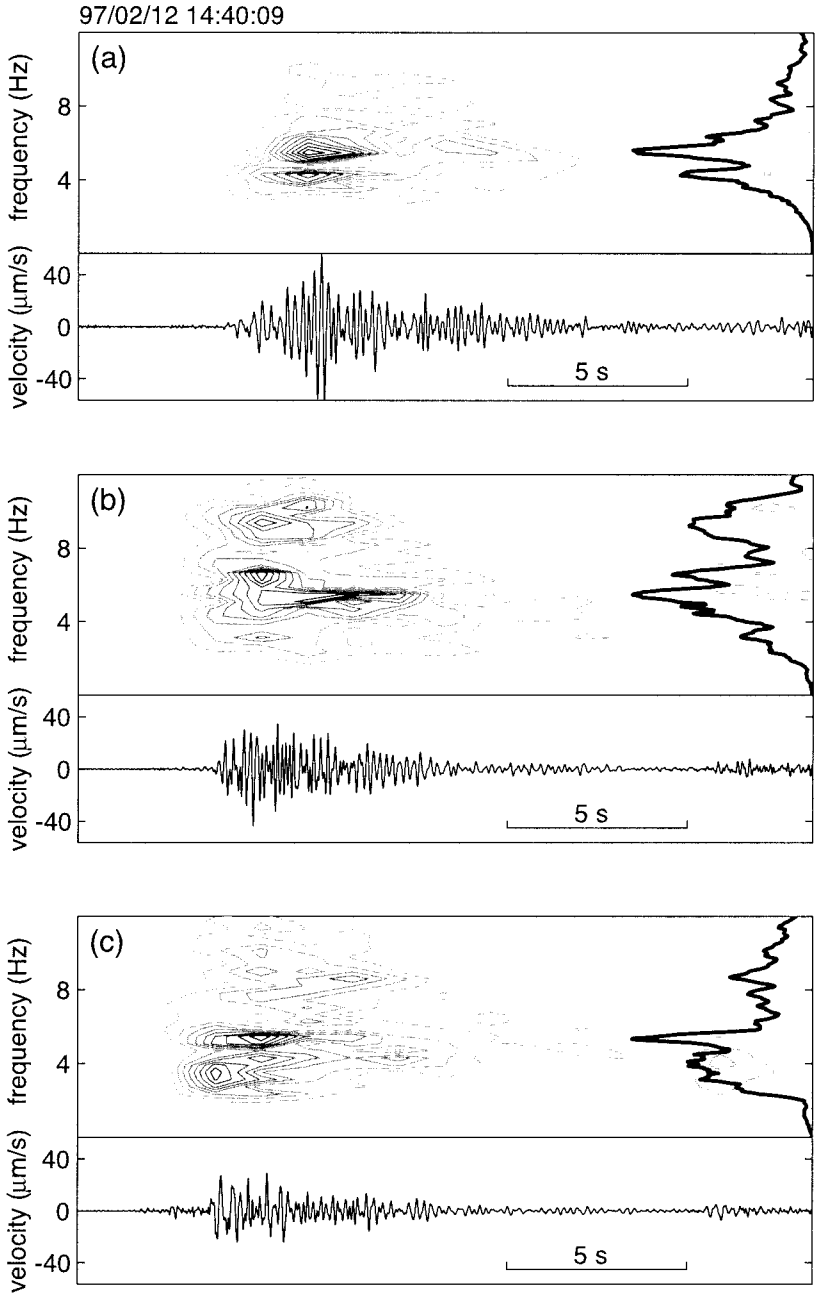

Figure 3. Vertical component seismograms and spectrograms of a LP event recorded at stations (a) D00, (b) E00, and (c) F21 (see Figure 1c). The sliding window length used for the spectrograms is 2.56 s. The bold curve on the right of the spectrograms is the normalized amplitude spectrum calculated over a window of 20.48 s (the entire trace shown) and smoothed using a running average procedure.

stacked slowness power appears, coincident with the first arrival of the event. The power remains high for a few seconds and then decreases through the end of the window, indicating that the wave field loses coherency. The azimuth remains stable and with small errors during the interval of enhanced power. The apparent slowness shows either small values at the beginning of the window and then a gradual increase or higher values that remain approximately constant within the first-arrival window. The former behavior is most likely due to the arrival, late in the window, of surface waves generated along the path between the source and the array that might not be detected in the latter. The errors, both for azimuth and slowness, increase along the window, in correspondence with the decay in power. For tremor we find the same characteristics, except that the stacked slowness power shows a slow increase trend instead of a sharp step.

We averaged the values of azimuth and slowness within the first-arrival window, using the error as a weighting factor in order to enhance the results with smaller errors. We used weighting functions in the forms $[1 - (\Delta\phi_i/\phi_{\mathrm{lim}})^n]$ and $[1 - (\Delta s_i/s_{\mathrm{lim}})]^n$, respectively, in which $\Delta\phi_i$ and Δs_i are the errors corresponding to the ith sample, ϕ_{lim} and s_{lim} are the maximum expected errors (360° and 2 s/km, respectively), and n is an exponent selected to enhance the difference between the

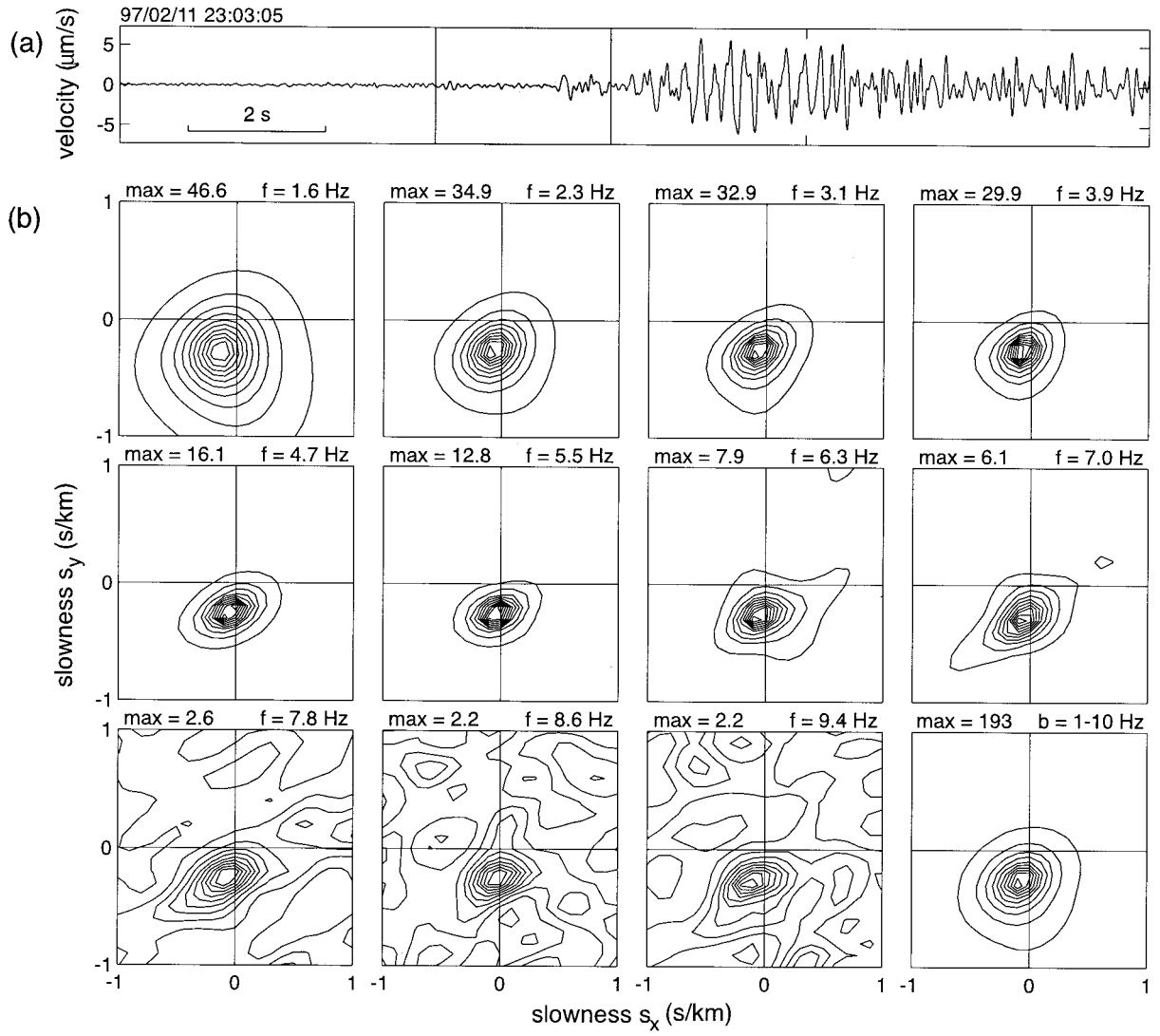

Figure 4. (a) Seismogram of a LP event recorded at station D00. The shading indicates the time window used for the frequency-slowness analysis whose results are shown in Figure 4b. (b) Frequency-slowness power spectra corresponding to the window shown in Figure 4a. The spectra are obtained for 11 frequency bands. The focusing frequency f and maximum frequency-slowness power, max, are indicated at the top of each spectrum. The stacked slowness power spectrum is shown at the bottom right and is labeled by total bandwidth b instead of focusing frequency.

low- and high-error solutions. We selected $n = 3$ for both LP events and tremor. The error associated with the average value of either slowness or azimuth is determined as the average of the errors. For the azimuth, which is generally stable within the first arrival window, this is a good estimate of the error. For the apparent slowness, however, we further consider the dispersion of the results, including the error limits, to obtain a better estimate of the range of variation of the solution.

Figures 5 and 6 show examples of analyses for a LP event and tremor sample, respectively. The parameters s_0 and ϕ_0 [see *Almendros et al.*, this issue, equation (4)] represent the apparent slowness and propagation azimuth of the wave field, respectively, obtained from frequency-slowness analyses of array data. Figures 5d and 6d show the average values of azimuth and slowness, as well as the error ranges, within the selected windows. The map view in Figures 5d and 6d provides an initial rough glimpse of the epicentral source region defined by the overlap of the shaded azimuthal wedges. As can be seen in Figures 5 and 6, these wedges overlap only slightly, partly because waves propagating in a heterogeneous medium do not follow a straight path. This issue is discussed in detail in section 5.

4.3. Results

Using the procedure described in section 4.2, we have obtained azimuths and apparent slownesses at the three antennas for 1129 LP events and 147 samples of tremor. Figure 7 shows histograms of apparent slowness and rose diagrams of azimuth for all the analyzed seismicity. The average azimuths and slownesses for LP events resolved with the D, E, and F antennas are 201, 167, and 360° and 0.44, 0.75, and 0.30 s/km, respectively. The average values for tremor are 201, 173, and 354° and 0.58, 1.04, and 0.27 s/km, respectively. The azimuths and slow-

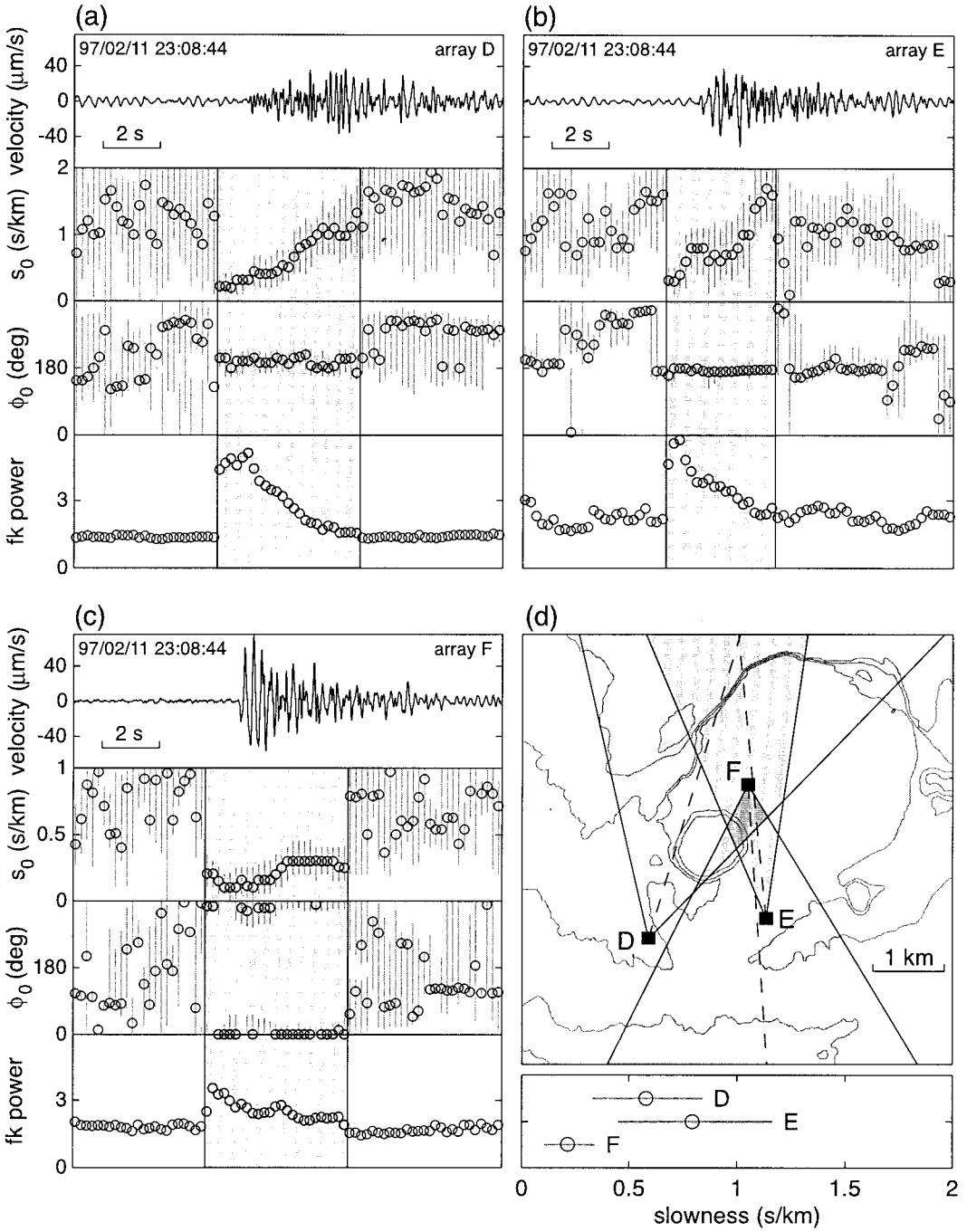

Figure 5. (a, b, c) Examples of results obtained from frequency-slowness analyses of an LP event recorded at antennas D, E, and F, respectively. From top to bottom, the seismogram recorded at a selected array site, the apparent slowness, azimuth, and peak stacked slowness power determined at the array are shown. Shading marks the first-arrival window (see text for explanations). (d) Graphic summary of the frequency-slowness results. (top) Map showing a tentative epicentral region defined by the overlap of the shaded wedges. These wedges represent the back azimuthal spreads resolved by the arrays. The dashed lines indicate the average back azimuths determined over the first-arrival windows. (bottom) Average slowness determined in the first-arrival window at each antenna.

nesses show little variation from event to event, and their distributions show only one peak, which suggests a common source region. The azimuths and slownesses are similar for both LP events and tremor. The average tremor slownesses are slightly higher, suggesting that the sources corresponding to the analyzed tremor samples are shallower on average than those of LP events.

It is worth noting the anomalous behavior of the slownesses observed at the E antenna as compared to those seen at the D and F antennas. The slownesses observed at E are consistently

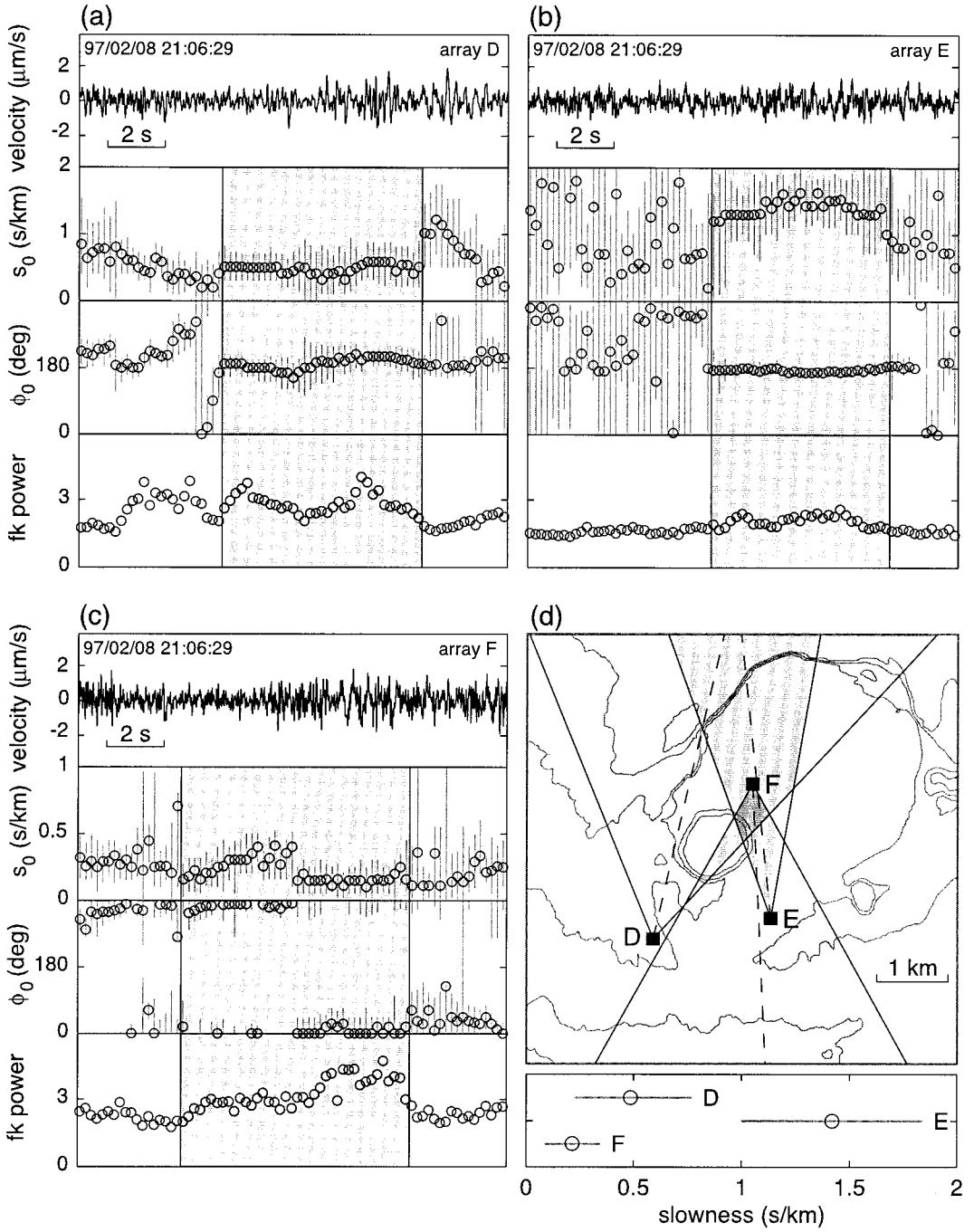

Figure 6. Same as Figure 5 for a sample of volcanic tremor.

higher, for both LP events and tremor, even when the source-array geometry does not seem to be very different. This could be an effect of either the shallow structure beneath the array or the heterogeneities along the ray path.

The magnitudes of the azimuth and slowness errors are roughly independent of the azimuth, showing that the directional responses of the antennas are homogeneous. However, errors strongly depend on the apparent slowness. In particular, the azimuth is better constrained when the slowness is high. The best resolving antennas, based on the average azimuthal errors, are, in this order, F, E, and D. There is no obvious explanation for this if we compare the array configurations because the D antenna actually represents the most dense configuration of sensors and has an aperture intermediate between the E and F array apertures. However, data recorded on the D antenna are consistently more emergent and show a lower signal-to-noise ratio than the data recorded on the other two antennas.

5. Source Location and Extent

In this section we apply the probabilistic method of *Almendros et al*. [this issue] to locate the source of the selected LP events and tremor. This method is based on a comparison between the slowness vectors obtained from frequency-slowness analyses of array data and a slowness vector model.

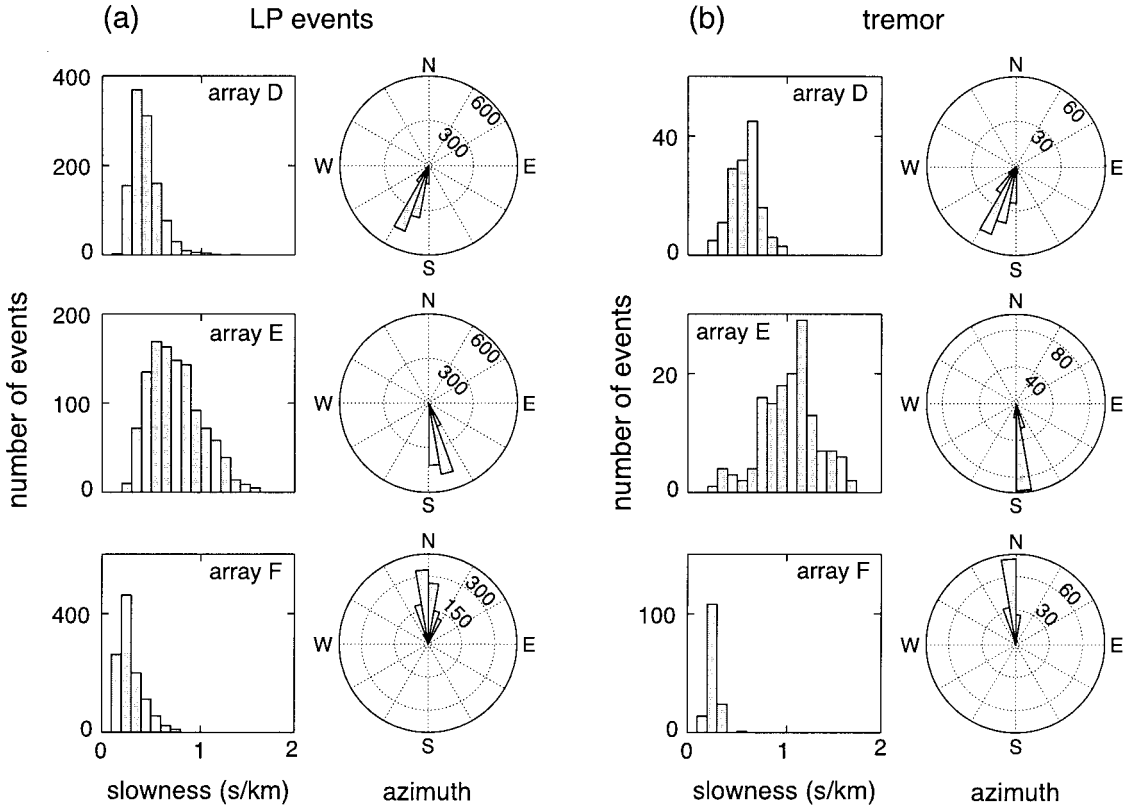

Figure 7. Histograms of apparent slownesses and rose diagrams of propagation azimuths obtained for (a) 1120 LP events and (b) 147 samples of tremor at the (top) D, (middle) E, and (bottom) F antennas. The widths of the bins are 0.1 s/km for slowness and 10° for azimuth.

The method provides an estimate of the source location and its associated error and a parameter called location quality, which is a measure of the goodness of the solution. *Almendros et al.* [this issue] define a restricted geometric slowness vector model that uses only azimuthal information to locate the epicenter and also present a synthetic slowness vector model that includes the effects of both topography and three-dimensional (3-D) velocity structure in the slowness vector estimates. The synthetic model is defined for a volume of 2.40 × 2.40 km in horizontal dimensions and 0.64 km in vertical extent (Figure 1b). The origin of coordinates is located at 19°24.5′N and 155°17.0′W at an elevation of 1088 m on the floor of the Halemaumau pit crater. All the coordinates we refer to in the following discussion are expressed as distances measured eastward, northward, and downward from this origin. The geometric model is used to determine a preliminary epicenter, and the synthetic model is applied to obtain a 3-D hypocenter location (see *Almendros et al.* [this issue] for an elaboration of these models).

5.1. Preliminary Epicenter Location: Geometric Model

As an illustration of what can be achieved with a simple slowness vector model, we estimated a preliminary epicenter using the restricted geometric model. The method is a refinement of the crude location method depicted in Figures 5d and 6d. In Figures 5d and 6d the epicenter was intuitively defined as the region within which all three azimuthal wedges overlap. Now we proceed to quantify this overlap by using azimuthal probability distributions.

Plate 1 shows an example of epicenter location determined for one LP event using the geometric model. Plates 1a–1c show the spatial probability distributions of azimuths corresponding to each of the three arrays. Plate 1d is the combined source location probability. The maximum probability occurs at (120,760) m, northeast of Halemaumau, where we fix the epicenter for this event. The location quality is 0.82. As an error limit, we use the contour representing 80% of the maximum probability, which yields a region with size of about 0.2 × 0.5 km.

The application of this method to all the LP events and tremor samples provides preliminary epicenters for the LP seismicity. All the epicenters are located near the eastern edge of Halemaumau. To determine the most active epicentral regions, we stacked the probabilities contained within the 80% contours of all the located seismicity. In this procedure, every event is weighted according to its location quality, so that low-quality events do not affect the stack unless many of them are located at the same point. The resulting probability distributions for LP events and tremor are shown in Plate 2. Almost all the activity occurs within a north-south elongated region immediately northeast of the Halemaumau crater. For both LP events and tremor the maximum probability occurs at (160,800) m. The size of the source region may be estimated by defining a minimum probability level. Below that level, we think that there is insufficient activity to consider the point as part of the source region. We select a level representing 5% of the maximum stacked probability (the white contour in Plate 2). The 5% contour bounds an epicentral region with size of

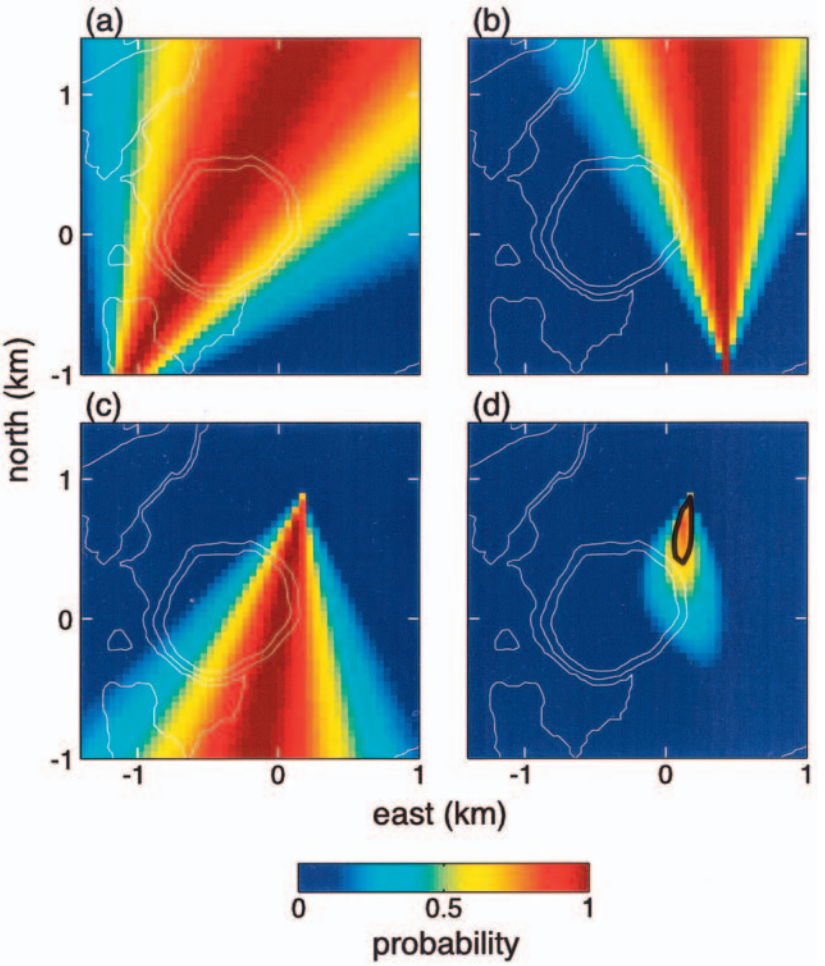

Plate 1. Epicenter location of one LP event obtained from the restricted geometric model. (a,b,c) Spatial probability distributions for azimuth at arrays D, E, and F, respectively. (d) Spatial source probability (the product of the three azimuthal distributions), showing a narrow peak that we take as the epicenter location of the event. The bold black line is the contour at 80% of the maximum probability, which we take as a measure of the error of the solution.

approximately 0.8 × 1.1 km for LP events and 0.5 × 1.1 km for tremor.

5.2. Hypocenter Location: Synthetic Model

We now compare the slowness vector data to the synthetic slowness vector model of *Almendros et al*. [this issue] to obtain a more accurate source location of the analyzed seismicity. The slowness vector model was elaborated by performing frequency-slowness analyses of synthetic signals radiated by isotropic point sources. Each point source has a seismic moment of 10^{12} N m and a source-time function in the form of a cosine with frequency of 2 Hz [*Almendros et al*., this issue]. As the spectra of the LP data have main peaks in the range 2–6 Hz, the choice of a 2-Hz signal for comparison with the data may seem somewhat inappropriate. However, the coherency of the observed wave fields, as measured by the frequency-slowness power, is usually highest in the low-frequency bands centered at 1.6 and 2.3 Hz (see Figure 4). These are the bands that dominate the stacked slowness spectrum, and therefore the selection of a 2-Hz model for comparison is adequate for our purposes.

Plate 3 shows the location of the LP event previously determined with the geometric model (Plate 1) now obtained with the synthetic slowness vector model. Each panel pair shows a map view and a north-south, vertical cross section in the 3-D probability distributions. The cross sections contain the maximum of the spatial source location probability. Plates 3a–3c show the spatial probability distributions for azimuths obtained at each of the three antennas. The white dashed lines in the map views mark the average geometric back azimuths and give a measure of the bias due to the effects of topography and structure, which can be quite large (up to 10°). Plates 3d–3f show the spatial probability distributions for slownesses obtained at each antenna.

The distribution corresponding to the E antenna is blank because of the anomalously high slowness values obtained at this antenna from frequency-slowness analyses. The slownesses measured at array E are excessively large compared to those measured at the other antennas (see Figure 7), and our synthetic model cannot account for those estimates. An explanation for these anomalies could be a very local path or site effect caused by a shallow structure that is too small to be resolved by the tomographic inversion of *Dawson et al*. [1999]. Antenna E lies on top of a shallow ponded pahoehoe flow, while antenna F lies on more consolidated rock, and antenna D sits on a sandy hill. The high density of vertical and horizontal cracks

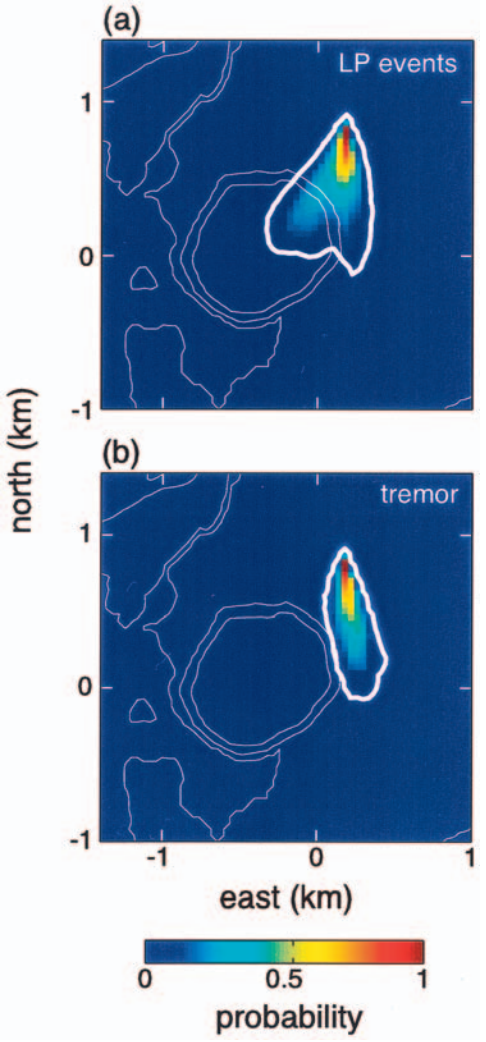

Plate 2. Stacked probability for epicenters obtained from the restricted geometric model for all the analyzed (a) LP events and (b) tremor. The bold white line is the contour representing 5% of the maximum stacked probability. We use this contour to define the source dimensions.

observed in the basalt layer beneath antenna E may have contributed to the anomalous response of this antenna. For this reason, we neglect the information on apparent slowness provided by antenna E and use only the slownesses determined at the other two antennas.

Plates 3g–3i show the combined azimuthal probability, combined slowness probability (from D and F only), and total probability distribution including azimuth and slowness (the spatial source probability). The maximum probability is located northeast of Halemaumau at (80, 640, 80) m. The location quality is 0.90, and the size of the error region is approximately 0.2 × 0.4 × 0.2 km.

Most of the hypocenters of the LP events are located within that same region (Plate 3i). Specifically, 857 hypocenters are located northeast of Halemaumau at depths shallower than 200 m. A subset of 132 events is located at depths near 400 m directly below Halemaumau (Plate 4a), while another group of 131 events is located in a shallow region extending southeastward from beneath the floor of Halemaumau (Plate 4b). Of the entire data set considered, only nine events were found to be located near the edges or outside of the domain outlined by the box in Figure 1b, and these are not considered to be part of the LP source region. For the tremor, all but one of the 147 analyzed samples represent shallow sources located in a region that coincides exactly with the most active source region of LP events. The remaining sample represents a source located slightly deeper beneath this zone. In all cases, the 80% probability surfaces that we take as a measure of the error in the locations generally fit within a sphere with radius of 200 m.

The location qualities (LQ) for the 1120 events within the LP source region range from small numbers (close to 0 for really ill-conditioned events) to high levels (near 1), with an average of 0.6 for the entire data set. It is worth noting that the spatial probability distributions determined for low-LQ events are the same as for well-located events. This gives confidence in the low-LQ results. The method seems to work well even in the worst-case situations. Although the errors are obviously larger in such cases, we still obtain an estimate of the source position. This clearly demonstrates the strong resolving power of seismic antennas in analyses of shallow LP seismicity, as compared to the poor capabilities of conventional networks for locating this type of seismicity.

As in section 5.1, we stack the spatial source probability contained within the 80% probability surfaces for the LP events and for the tremor to obtain a picture of the overall source region that produced the February 1997 seismic swarm. We define the source regions of the two types of seismic signals as the volumes contained inside the surfaces corresponding to 5% of the maximum of the stacked source location probability. The choice of 5% is conservative enough to include all the located hypocenters and yields maximum constraints on the sizes of the source regions.

Plate 5a shows the source region of LP events. The most active zone is located just outside the northeast edge of the Halemaumau pit crater, at depths around 150 m (region A in Plates 5b and 5c). This region includes 857 of the 1120 LP event hypocenters. Another 132 events are clustered in a secondary source region at depths of ~400 m below the northeast quadrant of Halemaumau (region B in Plate 5c). A third, less dense cluster that includes 131 hypocenters, is located at depths shallower than 200 m in an elongated zone extending from the northeast quadrant of Halemaumau to a region immediately southeast of Halemaumau. This region is seen in Plate 5a as the arm extending southeast from Halemaumau; the northwest extent of this arm is visible in the cutaway view in Plate 5c (region C). The individual event clusters are not completely separated, and a few events do occur between these clusters, suggesting a connection between the different zones of high activity and providing a rough glimpse of the three-dimensional structure of the overall source region. However, our model is not accurate enough to provide further resolution of those details. For the tremor the method reveals a single source region (Plates 5d and 5e) coincident with the most active source region of LP events (compare regions A and A′ in Plate 5). This result demonstrates the strong relation that exists between the two types of activity. The dimensions of the source regions are approximately 0.6 × 1.0 × 0.5 km for LP events and 0.2 × 0.5 × 0.2 km for tremor, with volumes of 0.09 and 0.01 km^3, respectively.

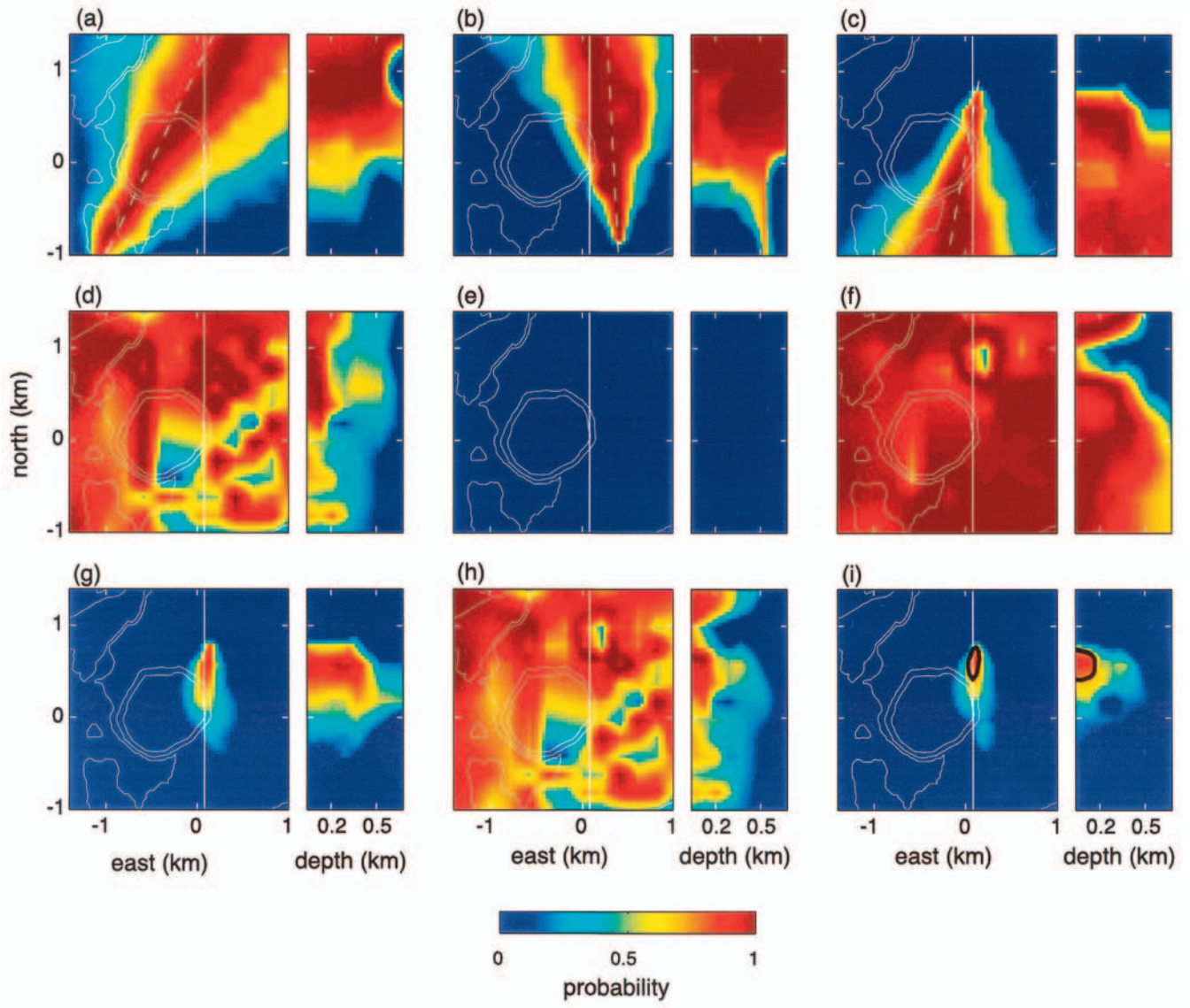

Plate 3. Spatial probability distributions used in the source location procedure for one LP event (same event as in Plate 1) using the synthetic slowness vector model. Each panel pair shows (left) a horizontal slice through a probability distribution at 40 m depth in the slowness model and (right) a north-south vertical cross section, whose position is marked by the white line in the map view. (a,b,c) Probability distributions for azimuths obtained at arrays D, E, and F, respectively. The white dashed lines show the average geometric back azimuths of the waves detected by each antenna. (d,e,f) Probability distributions for slownesses obtained at arrays D, E, and F, respectively. The probability distribution for slowness obtained at the E antenna (Plate 3e) is not used (see text for explanations). (g) Combined probability for azimuth, the product of Plates 3a, 3b, and 3c. (h) Combined probability for slowness, the product of Plates 3d and 3f. (i) Spatial source probability, including both azimuth and slowness information. The bold black lines are contours of the surface at 80% of the maximum probability. We take these contours as a measure of the error of the solution.

6. Discussion and Conclusions

6.1. Considerations About the Method

The data we analyzed consist of a typical swarm of LP seismicity, with bursts of energy in the form of LP events overriding a background tremor. We have located both individual events and tremor. The source locations are obtained in a probabilistic sense by comparing the slowness vectors derived from frequency-slowness analyses of array data with a synthetic slowness vector model. Individual event locations are estimated to have an error of ±200 m. By stacking over a thousand LP events and ~150 samples of tremor, we obtained a robust 3-D picture of the source regions.

The slowness model that we used was calculated using synthetic signals that include the effects of topography and 3-D velocity structure on the propagating wave fields [*Almendros et al.*, this issue]. A major limitation of this slowness model stems from the resolution of the 3-D velocity structure. The velocity structure that we used was obtained by interpolating a tomography model for Kilauea with a 500-m spatial resolution [*Dawson et al.*, 1999] over a 40-m equally spaced grid. The Dawson et al. model is probably the most

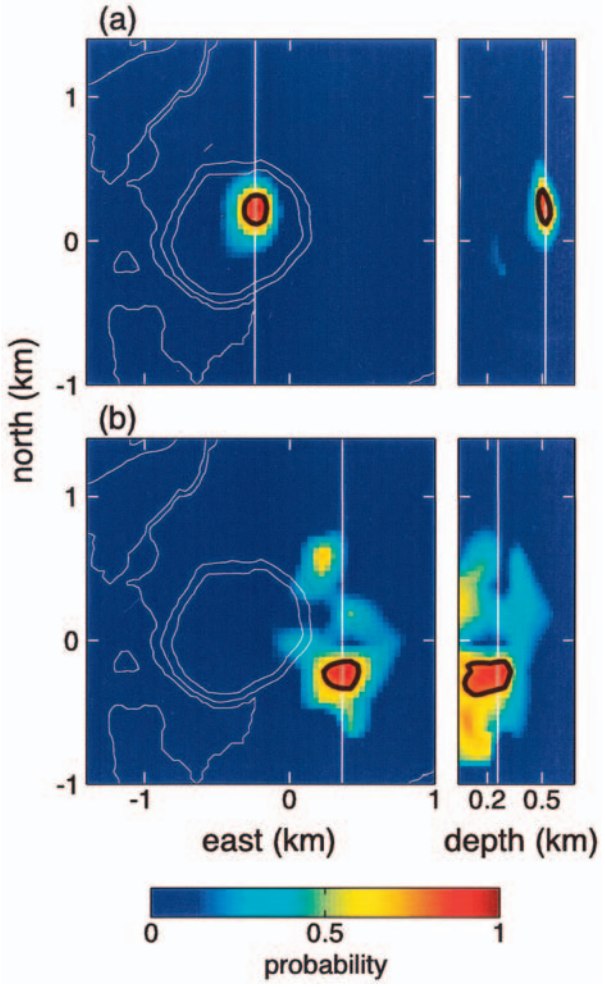

Plate 4. Same as Plate 3i for individual LP events located in other source regions around Halemaumau. The map views represent horizontal sections of the source location probability distributions at the source depth, as indicated by the white lines in the vertical cross sections. (a) Event located at depth of 520 m beneath the northeast quadrant of Halemaumau. (b) Event located at depth of 260 m, southeast of Halemaumau.

precise image of the 3-D velocity structure of Kilauea available today, but this level of detail is still not sufficient to explain all the rich variety of behavior found in the data. For example, we observed that the slowness increases with time from the onset of the LP events to values above 1 s/km, a pattern typical of wave dispersion. The synthetic signals cannot match this behavior at the frequency of 2 Hz considered for the source, but using higher frequencies for synthetic signals is not realistic unless we improve our knowledge of the medium.

This need for a higher-resolution tomographic model limits the applicability of the method to volcanoes other than Kilauea because velocity structures are not yet well known for most volcanoes around the world. However, the number of volcanoes being imaged by tomography is slowly increasing [e.g., *Benz et al*., 1996; *Villaseñor et al*., 1998]. The growing number of high-resolution tomographic models may transform the procedure described here and by *Almendros et al*. [this issue] into a widely used tool for locating LP seismicity.

The application of our method to array data allows us to determine source locations not only for events that have impulsive phases and can be located with a distributed seismic network but also for noisy or very emergent events and for tremor, neither of which can be located by conventional phase pick techniques. This is a very important point because most of the LP seismicity observed at volcanoes around the world comprises emergent, spindle-shaped LP events riding on a sustained background of tremor. Reliably locating the source of this LP seismicity is critical to understanding the physical processes underlying this activity and to quantifying their role in the overall dynamics of volcanoes.

6.2. Considerations About the Source

The source region imaged from our analyses encompasses a small volume near the northeastern edge of the Halemaumau pit crater. That all the February 1997, LP activity was generated in this region is not surprising. This is a highly fractured region where several eruptions have occurred over the past 30 years. For example, this site was covered by lava flows during short-lived caldera eruptions in August 1971, November 1975, and April 1982 (HVO web site, http://hvo.wr.usgs.gov/kilauea/history, 2000). The surface area around Halemaumau, including the LP source region, is visibly altered and shows the effects of volcanic gas emissions; it is hot and steaming at several locations.

The percentage of LP events that we have analyzed is very high. We counted seismic events by applying a detection threshold of 0.6 μm/s to the amplitude of the low-pass-filtered record obtained at station F21 (Figure 1c). This yields a count of 47 events for the 50 min shown in Figure 2. In this manner, 1356 events were detected during the 23 hours of data considered in our analysis. This number compares well with the total of 1129 events analyzed. Our data set corresponds to 83% of the total activity, and accordingly, we consider our results to be representative of the overall behavior of the swarm. For tremor, however, the 147 analyzed samples might not be representative of the overall tremor activity. We had to restrict ourselves to those samples coherent enough to allow their location using the antennas and recorded during time periods quiet enough for them to show up. Therefore we leave out a great portion of the tremor, and there could be other source regions apart from the one imaged here.

A common source is usually inferred for LP events and tremor based on similarities observed in their spectra, their times of occurrence, and the spatial attenuation of their amplitudes [*Koyanagi et al*., 1987; *Chouet*, 1988; *Chouet et al*., 1994]. *Almendros et al*. [1997] used array techniques to demonstrate that the apparent slowness vectors for both individual LP events and tremor recorded at Deception Island, Antarctica, were exactly the same, a finding indicative of a common source region. At Kilauea we have located both the source of LP events and the source of tremor and have found that the latter is coincident with the most active source region of LP events. This observation is in harmony with the idea that the two types of events are generated by similar fluid dynamical processes but with different excitation mechanisms producing either discrete (LP event) or sustained signal (tremor) [*Chouet*, 1996]. We did not identify any tremor episodes originating in the regions characterized by weaker LP event activity.

Several fluids may be related to the generation of LP seismicity in volcanoes, including bubbly magma or bubbly water and gas-gas or gas-ash mixtures [*Kumagai and Chouet*, 1999, 2000]. In view of the shallow depths determined for the seismic

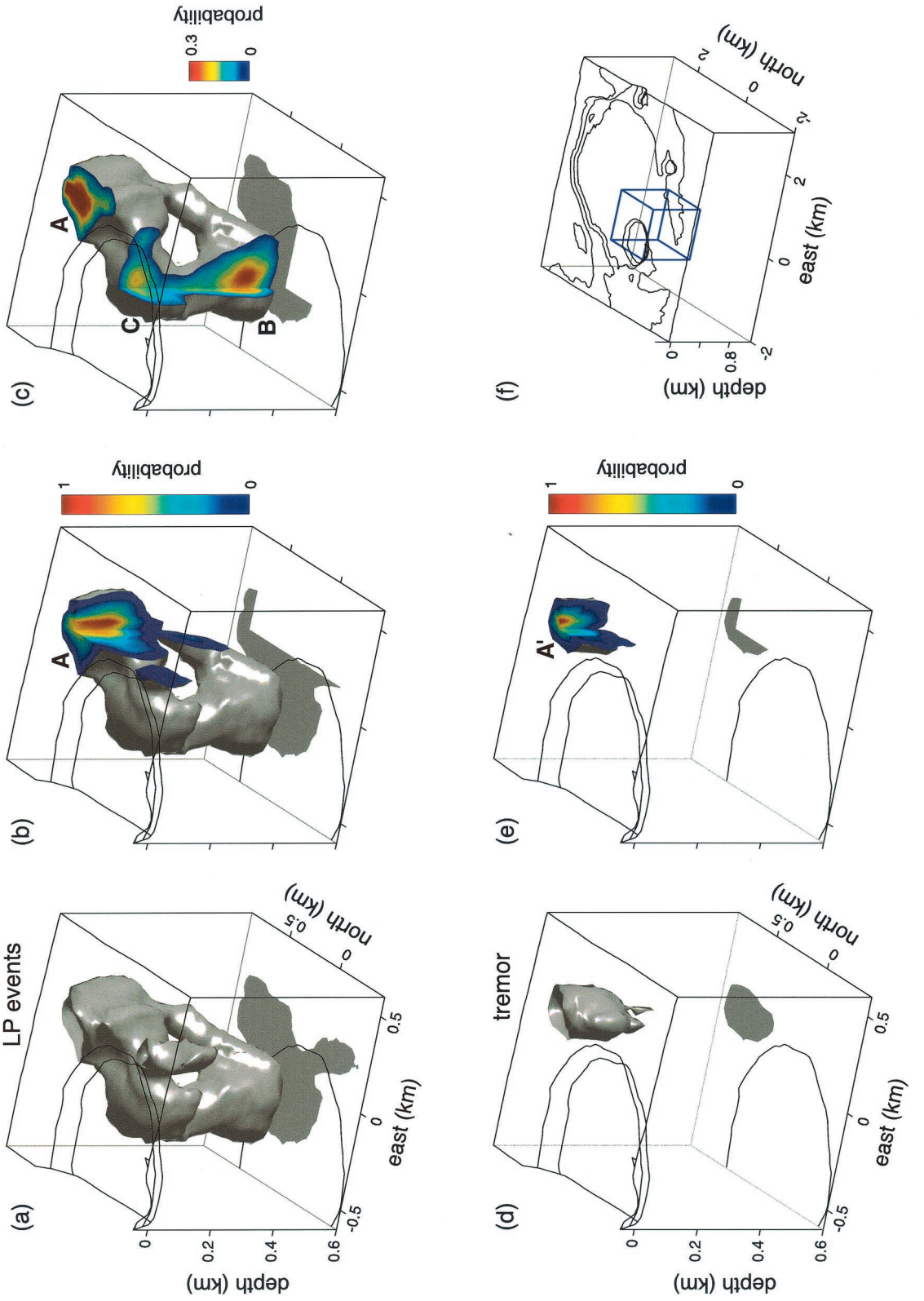
(a)
LP events
depth (km)
east (km)
north (km)
(b)
probability
A
(c)
probability
A
C
B
(d)
tremor
depth (km)
east (km)
north (km)
(e)
probability
A'
(f)
depth (km)
east (km)
north (km)

Plate 5. (a) A 3-D view of the source region of LP events. The source region is estimated as the region inside the surface corresponding to 5% of the maximum of the stacked source location probability obtained for the 1120 LP events considered in our analysis. The horizontal projection of the source region and rim of the Halemaumau pit crater shown on the floor of the cube helps to provide a better idea of the spatial distribution of seismicity. (b) Cutaway view of the source region, showing the most active source zone located northeast of the Halemaumau pit crater (A). (c) Secondary clusters of hypocenters also present at two depths beneath the crater (B,C). The maximum of the color scale is 0.3. Accordingly, the probability is saturated in the main source region shown in Plate 5b. (d) A 3-D view of the source region of tremor obtained from the surface of 5% of the maximum stacked probability corresponding to the 147 tremor samples considered. (e) Cutaway view of the stacked source location probability, showing that there are no subregions and that the maximum probability occurs in a region that coincides with the most active zone of LP event generation (A'). (f) General view of the summit region. The blue cube shows the boundaries of the region extracted in Plates 5a–5e.

source regions and the known existence of a large-scale hydrothermal system permeating the entire volcanic edifice and in particular the summit caldera [*Ingebritsen and Scholl*, 1993] the fluids that may reasonably be viewed as responsible for the generation of the LP seismicity near Halemaumau are either mixtures of water and gas bubbles or gas-gas mixtures. The location and extent of the source region strongly point to a hydrothermal origin for the LP swarm. In analyzing one LP event originating in the same source region a year earlier, *Saccorotti et al*. [2001] determined that the characteristics of the dominant spectral peak of this event were compatible with the excitation of a crack with scale length of 20–100 m and an aperture of a few centimeters, filled with bubbly water. The dominant frequencies of LP events analyzed in the present study are higher than that of the LP event analyzed by *Saccorotti et al*. [2001], suggesting that the fluid involved in the February 1997 swarm may have been dominated by a gas phase [*Kumagai and Chouet*, 2000].

Ohminato et al. [1998] performed waveform inversions of very long period (VLP) signals associated with a magmatic surge at Kilauea on February 1, 1996, and identified a magma conduit at a depth of 1 km below the northeast edge of Halemaumau. Their results point to a crack-like source, which acts like a buffer to the flow of magma from beneath the summit of Kilauea to the East Rift Zone. The typical behavior of the crack consists of a slow (1–3 min long) inflation phase, followed by a rapid (5–10 s long) deflation, producing a sawtooth signal in the VLP range. Each sawtooth corresponds to a batch of 1000–4000 m^3 of magma passing through the crack. *Chouet and Dawson* [1997] analyzed VLP signals recorded in February 1997 and determined a source location for those signals that is essentially the same as that determined by *Ohminato et al*. [1998], although the source mechanism imaged by *Chouet and Dawson* [1997] is different. In this study, we have found that the source of the February 1997 LP seismicity is located directly above the magma conduit system imaged from the VLP signals in 1996 and 1997, suggesting that LP seismicity may reflect the response of the hydrothermal system to enhanced degassing resulting from increased magma transport in the deeper magma conduit. The deflation and reinflation of Kilauea's summit, and attendant brittle failure of rock in the lid capping the magma conduit, may have allowed the upward transport of magmatic gases and heat through the fractured medium to shallow depths beneath the surface, where the hot gases heated and activated the hydrothermal system. Boiling groundwater and steam, and/or unsteady gas flow, induced pressure perturbations that triggered the resonance of fluid-filled cracks which produced the seismic signatures observed during the LP swarm. We note that there are no LP sources at depths below 500 m, which suggests either an absence of water and/or steam below 500 m, or a lack of measurable pressure fluctuations in the streaming hot gases at those depths.

The limited spatial extent of the most active cluster of LP events (region A in Plate 5) might suggest the presence of a single, repeatedly activated source. In that case, all the LP events originating from the repeated excitation of the same fluid-filled crack should show very similar seismic signatures. Similarities in the waveform of LP events have been observed in several volcanoes around the world [*Chouet et al*., 1994; *Poupinet et al*., 1996; *Ibáñez et al*., 2000], demonstrating that this is often the mechanism of LP swarm generation. However, the waveforms of the LP events analyzed in this paper are quite diverse. This suggests that the source probably consists of a

dendritic system of cracks and fissures, in which different cracks are excited at different times during the swarm.

Sutton et al. [2001] determined that there is a positive correlation between summit SO_2 emissions and the occurrence of shallow, ~5-Hz seismic events, routinely classified as caldera events by HVO. This relationship between gas emissions and shallow seismic activity supports our hypothesis that the analyzed LP swarm was triggered by the enhanced transport of gas and heat from the magma conduit below Halemaumau. Moreover, this correlation suggests that all the shallow earthquakes usually classified by HVO as caldera events may really be LP events generated by the resonance of fluid-filled cavities excited by the degassing of magma as it reaches its shallowest point beneath the summit of Kilauea before being shunted into the rift zones.

Despite the usually gentle character of Kilauea eruptions, the interaction between the magmatic and hydrothermal systems is known to lead, on occasions, to explosive phreatic eruptions [*Decker and Christiansen*, 1984; *Dvorak*, 1992]. The most recent phreatic eruption took place in Halemaumau in May 1924. Phreatic eruptions have occurred several times in Kilauea's history, as evidenced in pyroclastic deposits [*McPhie et al*., 1990; *Dzurisin et al*., 1995; *Mastin*, 1997]. Therefore the study of shallow, hydrothermal-related seismicity is a very important aspect of the assessment of volcanic hazards at Kilauea and other volcanoes worldwide.

Acknowledgments. We are grateful to Y. Ida, T. Iwasaki, N. Gyoda, J. Oikawa, M. Ichihara, Y. Goto, T. Kurihara, M. Udagawa, and K. Yamamoto of the Earthquake Research Institute, University of Tokyo; K. Yamaoka, M. Nishihara, and T. Okuda of Nagoya University; H. Shimizu and H. Yakiwara of Kyushu University; E. Fujita of the National Research Institute for Earth Science and Disaster Prevention, Tsukuba; T. Ohminato of the Geological Survey of Japan, Tsukuba; S. Adachi of Hakusan Corporation; C. Dietel and P. Chouet of the U.S. Geological Survey, Menlo Park; P. Okubo, A. Okamura, M. Lisowski, M. Sako, K. Honma, and W. Tanigawa of the U.S. Geological Survey, Hawaiian Volcano Observatory; S. McNutt, D. Christensen, and J. Benoit of the University of Alaska Fairbanks; and S. Kedar of the California Institute of Technology, Pasadena, for their participation in the field experiment. In particular, we wish to thank Y. Ida, whose exceptional organizational skills made this experiment possible. Funding for the experiment was provided by a grant from the Japanese Ministry of Education (Monbusho) to the Earthquake Research Institute of the University of Tokyo. We also thank Bob Page, Chris Stephens, Gaetano De Luca, Jesús Ibáñez, and Alan Linde for constructive comments and Bob Tilling for providing useful data and advice. The work by J. Almendros was partially supported by a Fellowship of the Spanish Ministry of Education.

References

Almendros, J., J. Ibáñez, G. Alguacil, and E. Del Pezzo, Array tracking of the volcanic tremor source at Deception Island, Antarctica, *Geophys. Res. Lett*., *24*, 3069–3072, 1997.

Almendros, J., J. M. Ibáñez, G. Alguacil, and E. Del Pezzo, Array analysis using circular wave-front geometry: An application to locate the nearby seismo-volcanic source, *Geophys. J. Int*., *136*, 159–170, 1999.

Almendros, J., B. Chouet, and P. Dawson, Spatial extent of a hydrothermal system at Kilauea Volcano, Hawaii, determined from array analyses of shallow long-period seismicity, 1, Method, *J. Geophys. Res*., this issue.

Benz, H. M., B. A. Chouet, P. B. Dawson, J. C. Lahr, R. A. Page, and J. A. Hole, Three-dimensional *P* and *S* wave velocity structure of Redoubt volcano, Alaska, *J. Geophys. Res*., *101*, 8111–8128, 1996.

Chouet, B., Resonance of a fluid-driven crack: Radiation properties and implications for the source of long-period events and harmonic tremor, *J. Geophys. Res*., *93*, 4375–4400, 1988.

Chouet, B., Long-period volcano seismicity: Its source and use in eruption forecasting, *Nature*, *380*, 309–316, 1996.

Chouet, B. A., and P. B. Dawson, Observations of very-long-period impulsive signals accompanying summit inflation at Kilauea Volcano, Hawaii, in February 1997 (abstract), *Eos Trans. AGU*, *76*(46), Fall Meet. Suppl., F429, 1997.

Chouet, B. A., R. A. Page, C. D. Stephens, J. D. Lahr, and J. A. Power, Precursory swarms of long-period events at Redoubt Volcano (1989–1990), Alaska: Their origin and use as a forecasting tool, *J. Volcanol. Geotherm. Res*., *62*, 95–135, 1994.

Chouet, B., G. Saccorotti, M. Martini, P. Dawson, G. De Luca, G. Milana, and R. Scarpa, Source and path effects in the wave fields of tremor and explosions at Stromboli Volcano, Italy, *J. Geophys. Res*., *102*, 15,129–15,150, 1997.

Chouet, B., G. De Luca, G. Milana, P. Dawson, M. Martini, and R. Scarpa, Shallow velocity structure of Stromboli Volcano, Italy, derived from small-aperture array measurements of strombolian tremor, *Bull. Seismol. Soc. Am*., *88*, 653–666, 1998.

Christofferson, E., The relationship of sea-floor spreading in the Pacific to the origin of the Emperor Seamounts and the Hawaiian Island Chain (abstract), *Eos Trans. AGU*, *49*, 214, 1968.

Clague, D. A., and G. B. Dalrymple, The Hawaiian-Emperor volcanic chain, part I, Geologic evolution, in *Volcanism in Hawaii*, edited by R. W. Decker, T. L. Wright, and P. H. Stauffer, *U.S. Geol. Surv. Prof. Pap*., *1350*, 5–54, 1987.

Dawson, P., B. Chouet, P. Okubo, A. Villaseñor, and H. Benz, Three-dimensional velocity structure of the Kilauea caldera, Hawaii, *Geophys. Res. Lett*., *26*, 2805–2808, 1999.

Decker, R. W., Dynamics of Hawaiian volcanoes: An overview, in *Volcanism in Hawaii*, edited by R. W. Decker, T. L. Wright, and P. H. Stauffer, *U.S. Geol. Surv. Prof. Pap*., *1350*, 997–1018, 1987.

Decker, R. W., and R. L. Christiansen, Explosive eruptions of Kilauea Volcano, Hawaii, in *Explosive Volcanism: Inception, Evolution, and Hazards*, pp. 122–132, Natl. Acad. Press, Washington, D.C., 1984.

Del Pezzo, E., S. De Martino, S. Gresta, M. Martini, G. Milana, D. Patane, and C. Sabbarese, Velocity and spectral characteristics of the volcanic tremor at Etna deduced by a small seismometer array, *J. Volcanol. Geotherm. Res*., *56*, 369–378, 1993.

Del Pezzo, E., M. La Rocca, G. Alguacil, J. Almendros, J. M. Ibáñez, J. Morales, A. García, and R. Ortiz, Observations of volcanic earthquakes and tremor at Deception Island, Antarctica, *Ann. Geofis*., *42*, 417–437, 1999.

De Luca, G., R. Scarpa, E. Del Pezzo, and M. Simini, Shallow structure of Mt. Vesuvius volcano, Italy, from seismic array analysis, *Geophys. Res. Lett*., *24*, 481–484, 1997.

Dvorak, J. J., Mechanism of explosive eruptions of Kilauea Volcano, Hawaii, *Bull. Volcanol*., *54*, 638–645, 1992.

Dzurisin, D., J. P. Lockwood, T. J. Casadevall, and M. Rubin, The Uwekahuna Ash Member of the Puna Basalt: Product of violent phreatomagmatic eruptions at Kilauea Volcano, Hawaii, between 2800 and 2100 years ago, *J. Volcanol. Geotherm. Res*., *66*, 163–184, 1995.

Eaton, J. P., and K. J. Murata, How volcanoes grow, *Science*, *132*, 925–938, 1960.

Ferrazzini, V., K. Aki, and B. Chouet, Characteristics of seismic waves composing hawaiian volcanic tremor and gas-piston events observed by a near-source array, *J. Geophys. Res*., *96*, 6199–6209, 1991.

Fiske, R. S., and W. T. Kinoshita, Inflation of Kilauea volcano prior to its 1967–68 eruption, *Science*, *165*, 341–349, 1969.

Goldstein, P., and R. Archuleta, Array analysis of seismic signals, *Geophys. Res. Lett*., *14*, 13–16, 1987.

Goldstein, P., and R. Archuleta, Deterministic frequency-wavenumber methods and direct measurements of rupture propagation during earthquakes using a dense array: Theory and methods, *J. Geophys. Res*., *96*, 6173–6185, 1991.

Goldstein, P., and B. Chouet, Array measurements and modeling of sources of shallow volcanic tremor at Kilauea Volcano, Hawaii, *J. Geophys. Res*., *99*, 2637–2652, 1994.

Gordeev, E. I., V. A. Saltykov, V. I. Sinitsin, and V. N. Chebrov, Temporal and spatial characteristics of volcanic tremor wave fields, *J. Volcanol. Geotherm. Res*., *40*, 89–101, 1990.

Heliker, C. C., and T. L. Wright, The Puu Oo-Kupaianaha eruption of Kilauea, *Eos Trans. AGU*, *72*, 521, 531, 530, 1991.

Ibáñez, J. M., J. Almendros, G. Alguacil, E. Del Pezzo, M. La Rocca, R. Ortiz, and A. García, Seismo-volcanic signals at Deception Island

volcano (Antarctica): Wave field analysis and source modeling, *J. Geophys. Res*., *105*, 13,905–13,931, 2000.

Ingebritsen, S. E., and M. A. Scholl, The hydrogeology of Kilauea Volcano, *Geothermics*, *22*, 255–270, 1993.

Klein, F. W., R. Y. Koyanagi, J. S. Nakata, and W. R. Tanigawa, The seismicity of Kilauea's magma system, in *Volcanism in Hawaii*, edited by R. W. Decker, T. L. Wright, and P. H. Stauffer, *U.S. Geol. Surv. Prof. Pap*., *1350*, 1019–1085, 1987.

Koyanagi, R. Y., B. Chouet, and K. Aki, Origin of volcanic tremor in Hawaii, part I, in *Volcanism in Hawaii*, edited by R. W. Decker, T. L. Wright, and P. H. Stauffer, *U.S. Geol. Surv. Prof. Pap*., *1350*, 1221–1257, 1987.

Kumagai, H., and B. Chouet, The complex frequencies of long-period seismic events as probes of fluid composition beneath volcanoes, *Geophys. J. Int*., *138*, F7–F12, 1999.

Kumagai, H., and B. Chouet, Acoustic properties of a crack containing magmatic or hydrothermal fluids, *J. Geophys. Res*., *105*, 25,493–25,512, 2000.

Lahr, J. C., B. A. Chouet, C. D. Stephens, J. A. Power, and R. A. Page, Earthquake classification, location and error analysis in a volcanic environment: Implications for the magmatic system of the 1989–1990 eruptions at Redoubt Volcano, Alaska, *J. Volcanol. Geotherm. Res*., *62*, 137–151, 1994.

Lockwood, J., R. Tilling, R. Holcomb, F. Klein, A. Okamura, and D. Peterson, Magma migration and resupply during the 1974 summit eruptions of Kilauea volcano, Hawaii, *U.S. Geol. Surv. Prof. Pap*., *1613*, 1999.

Mastin, L. G., Evidence for water influx from a caldera lake during the explosive hydromagmatic eruption of 1790, Kilauea Volcano, Hawaii, *J. Geophys. Res*., *102*, 20,093–20,109, 1997.

McNutt, S. R., Y. Ida, B. A. Chouet, P. Okubo, J. Oikawa, and G. Saccorotti, Kilauea Volcano provides hot seismic data for joint Japanese–U.S. experiment, *Eos Trans. AGU*, *78*(10), 105–111, 1997.

McPhie, J., G. P. L. Walker, and R. L. Christiansen, Phreatomagmatic and phreatic fall and surge deposits from explosions at Kilauea Volcano, Hawaii, 1790 A.D.: Keanakakoi Ash Member, *Bull. Volcanol*., *52*, 334–354, 1990.

Métaxian, J. P., P. Lesage, and J. Dorel, Permanent tremor of Masaya volcano, Nicaragua: Wave field analysis and source location, *J. Geophys. Res*., *102*, 22,529–22,545, 1997.

Moran, S. C., Seismicity at Mount St. Helens, 1987–1992: Evidence for repressurization of an active magmatic system, *J. Geophys. Res*., *99*, 4341–4354, 1994.

Ohminato, T., B. Chouet, P. Dawson, and S. Kedar, Waveform inversion of very long period impulsive signals associated with magmatic injection beneath Kilauea Volcano, Hawaii, *J. Geophys. Res*., *103*, 23,839–23,862, 1998.

Poupinet, G., A. Ratdomopurbo, and O. Coutant, On the use of earthquake multiplets to study fractures and the temporal evolution of an active volcano, *Ann. Geofis*., *39*, 253–264, 1996.

Ryan, M. P., R. Y. Koyanagi, and R. S. Fiske, Modeling of the three-dimensional structure of macroscopic magma transport system: Application to Kilauea Volcano, Hawaii, *J. Geophys. Res*., *86*, 7111–7129, 1981.

Saccorotti, G., B. Chouet, and P. Dawson, Wavefield properties of a shallow long-period event and tremor at Kilauea volcano, Hawaii, *J. Volcanol. Geotherm. Res*., in press, 2001.

Schmidt, R. O., Multiple emitter location and signal parameter estimation, *IEEE Trans. Antennas Propag*., *34*, 276–280, 1986.

Sutton, A. J., T. Elias, T. M. Gerlach, and J. B. Stokes, Implications for eruptive processes as indicated by sulfur dioxide emissions from Kilauea Volcano, Hawaii, 1979–1997, *J. Volcanol. Geotherm. Res*., in press, 2001.

Swanson, D. A., W. A. Duffield, D. B. Jackson, and D. W. Peterson, Chronological narrative of the 1969–71 Mauna Ulu eruption of Kilauea Volcano, Hawaii, *U.S. Geol. Surv. Prof. Pap*., *1056*, 1979.

Tilling, R. I., Fluctuations in surface height of active lava lakes during 1972–1974 Mauna Ulu eruption, Kilauea volcano, Hawaii, *J. Geophys. Res*., *92*, 13,721–13,730, 1987.

Tilling, R. I., and J. J. Dvorak, Anatomy of a basaltic volcano, *Nature*, *363*, 125–133, 1993.

Villaseñor, A., H. M. Benz, L. Filippi, G. De Luca, R. Scarpa, G. Patane, and S. Vinciguerra, Three-dimensional *P*-wave velocity structure of Mt. Etna, Italy, *Geophys. Res. Lett*., *25*, 1875–1978, 1998.

Wilson, J. T., Evidence from islands on the spreading of the sea floor, *Nature*, *197*, 536–538, 1963.

Wolfe, E. W. (Ed.), The Puu Oo eruption of Kilauea Volcano, Hawaii: Episodes 1 through 20, January 3, 1983, through June 8, 1984, *U.S. Geol. Surv. Prof. Pap*., *1463*, 1988.

J. Almendros, B. Chouet, and P. Dawson, U.S. Geological Survey, 345 Middlefield Road, MS 910, Menlo Park, CA 94025. (noba@usgs.gov)

(Received September 26, 2000; revised March 2, 2001;
accepted March 15, 2001.)